CHALMERS
UNIVERSITY OF TECHNOLOGY

A Wide Scanning Array of Connected Bowtie Antennas Suitable for Integration in Composite Sandwich Structures With Monte-Carlo

Downloaded from: https://research.chalmers.se, 2025-12-06 04:12 UTC

Citation for the original published paper (version of record):
Khanal, P., Yang, J., Ivashina, M. et al (2021). A Wide Scanning Array of Connected Bowtie Antennas Suitable for Integration in Composite
Sandwich Structures With Monte-Carlo Tolerance Analysis. IEEE Access, 9: 146691-146702.
http://dx.doi.org/10.1109/ACCESS.2021.3123439

N.B. When citing this work, cite the original published paper.

© 2021 IEEE. Personal use of this material is permitted. Permission from IEEE must be obtained for all other uses, in any current or future media, including reprinting/republishing this material for advertising or promotional purposes, or reuse of any copyrighted component of this work in other works.

(article starts on next page)

Received October 9, 2021, accepted October 25, 2021, date of publication October 27, 2021, date of current version November 4, 2021.

Digital Object Identifier 10.1109/ACCESS.2021.3123439

A Wide Scanning Array of Connected Bowtie Antennas Suitable for Integration in Composite Sandwich Structures With Monte-Carlo Tolerance Analysis

PRABHAT KHANAL[1], (Graduate Student Member, IEEE), JIAN YANG[1], (Senior Member, IEEE), MARIANNA IVASHINA[1], (Senior Member, IEEE), ANDERS HÖÖK[2], AND RUOSHAN LUO[2]

[1]Department of Electrical Engineering, Chalmers University of Technology, 41296 Gothenburg, Sweden
[2]Saab AB, 41276 Gothenburg, Sweden

Corresponding author: Prabhat Khanal (prabhat@chalmers.se)

This work was supported by the Sweden's Innovation Agency VINNOVA through an NFFP 7 - 2017 grant (2017-04871).

ABSTRACT A low-profile and wide-scan phased-array antenna of connected cross-bowtie elements is proposed. The design goals and considerations are based on the applications requiring the integration of a large array antenna with composite sandwich structures, such as antennas on aircraft. In a very large array environment (modelled approximately as an infinite array), the main beam of the proposed antenna can be steered up to $\pm 75°$ at azimuth and $\pm 15°$ at elevation over bandwidths of 10% and 25% with active reflection coefficients below -10 dB and -5 dB, respectively. A Monte Carlo analysis of critical manufacturing and alignment tolerances shows the desired performance is achieved with the cumulative distribution probability over 80% under the uniformly distributed random combinations of the tolerances. Experimental results of a 7×7 element array prototype agree well with the simulations of this small-scale array case. The experiments show that this small-scale prototype is capable of steering the beam within the range of $[-60°, 60°]$ at azimuth and $[-15°, 15°]$ at elevation with the predicted performance satisfying the targeted application requirements and mechanical constraints. The achieved combination of the wide beam steering performance, relatively low antenna profile, and suitability of its feeding structure for sandwiched electro-mechanical integration makes this design unique with respect to the previously published results.

INDEX TERMS Bowtie antenna, composite sandwich structure, connected array, fuselage integration, phased array.

I. INTRODUCTION

Phased array antennas are widely used in, for example, targets tracking in radars and digital beamforming in communication systems owing to their ability of high-speed beam scanning and multiple beam generation. Common choices for wide-scan phased array elements are tapered slot antennas (TSAs) [1], [2], non-exponential notch antennas [3], and other traveling wave antennas [4]. However, these antennas are often of high profile with the element height in the order of one wavelength, λ. An antenna profile refers to the antenna height from the ground plane to the top of antenna elements.

The associate editor coordinating the review of this manuscript and approving it for publication was Davide Comite.

Phased-array antennas have theoretically bound relationships between the elements height, relative bandwidth, and scan range [5]. In particular, the traditional $\lambda/4$ element height is optimal at broadside for typical narrow-band array antennas, while higher elements enable scanning at large off-broadside angles. The latter result is associated with the change of the current mode on the antenna structure, from a dipole type electrical current (at broadside) to a loop type current when scanning at wide angles [6]. Hence, thin array antennas, such as single-mode patch array antennas, cannot scan to wide angles, as compared to, for example, TSA element arrays.

An interesting example is PCB-based magneto-dipole antenna arrays [7], which have a low profile and wide scan

This work is licensed under a Creative Commons Attribution 4.0 License. For more information, see https://creativecommons.org/licenses/by/4.0/

range (up to ±76°), owing to their unique ability to support both dipole- and loop type currents. However, the relative bandwidth of such designs is in practice small (< 4.5%) and realized only for a linear array. Other types of phased-arrays of multi-mode antenna elements [8]–[10] employ multi-mode excitation at elements that varies with beam direction to achieve wide scan range up to ±64° in an 8 × 8 array [10]. However, they need a doubled or more number of ports and optimal combiners for each antenna element in the array, which increases the design complexity and cost significantly and it is quite difficult to extend to large arrays. A similar idea lies behind pattern reconfigurable linear or quasi-linear antenna arrays [11], [12], where PIN diodes are used to switch between different excitation points of the antenna to support the scan range up to ±75° (only for linear array). This active-feeding solution is also complex and costly, and only suitable for linear arrays.

Connected and tightly coupled arrays represent a special class of phased arrays that are capable of wide beam scanning thanks to the strong mutual coupling effects. A common choice of the antenna element type is a dipole, slot or Vivaldi antenna, as these are easy to be implemented in PCB technology and large-scale arrays. A particular challenge in such designs, however, is how to achieve a low-loss and compact mechanically-stable feeding structure of the array element [1], [13]–[15]. Another major challenge is the assembly of the array, including its critical transitions (e.g. inter-element, element-to-feed, ground plane interface, etc.). In most research publications, however, the assembly complexities are often omitted from the critical design considerations.

This paper presents a new type of connected antenna array comprising bowtie antenna elements that enables an ultra-wide beam steering range (i.e. up to ±75° for a planar large-scale array) over moderate bandwidth. A unique and important feature of this array is that it is of relatively low profile and implemented in PCB technology with a simple mechanically stable balun and antenna feeding structure. The latter makes it suitable for the integration in aircraft fuselage through joint electromagnetic-mechanical design in a sandwich structure.

The paper is organized as follows. Section II introduces the application requirements and design considerations. Section III describes the antenna design. Section IV presents the Monte-Carlo analysis of the manufacturing and assembly tolerances. Section V shows the experimental results of a 7×7 element array prototype. Concluding remarks are given in Section V.

II. APPLICATION REQUIREMENTS AND DESIGN CONSIDERATIONS

The present work aims to study the feasibility of a low-volume, lightweight, high endurance, wide-scanning sandwich structured fuselage integrated antenna array. The size of the whole antenna array shall be comparable to the size of the aircraft. Hence, reducing the weight and volume of the antenna will help to reduce its total weight, volume and drag. As a result of the fuselage integration, it is expected to have increased flight time, lower operating costs, and larger coverage. This type of design could be applied to surveillance, reconnaissance and early warning aircraft and satellites.

Subsections II-A and II-B briefly explain the concept of the fuselage integration and the sandwich structure respectively and subsection II-C discuss the design goals and considerations of the present work.

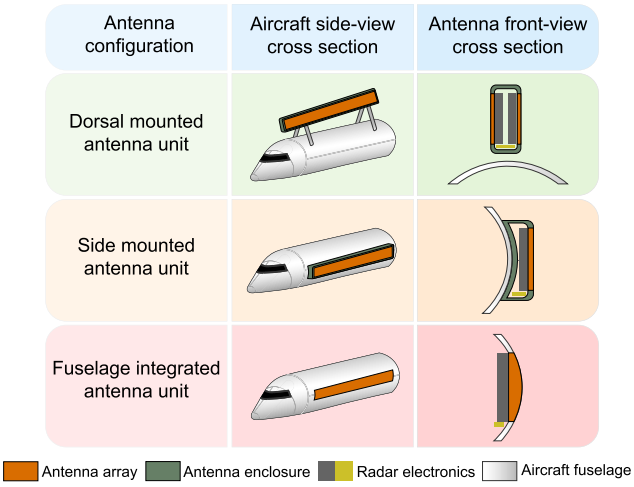

FIGURE 1. Body-wide antenna array structure integration solutions on an aircraft.

A. FUSELAGE INTEGRATION

Fig. 1 shows three possible integration solutions for a body-wide antenna array on an aircraft. The dorsal mounted units are stand-alone antenna arrays that are installed on top of an aircraft such as [16]. The side-mounted units are conformal antenna arrays installed on the sides of the conventional fuselage structure such as in [17], [18]. The key challenge of such on-aircraft array antennas is to realize a low-profile antenna design while enabling broad beam-scanning characteristics. This is because there are fundamental limitations on the maximum scan angle for a given antenna profile; thereby, array antennas with wide beam-scanning are often of high profile [5]. However, the high profile antenna arrays are not suitable as conformal arrays since they will create protrusions in the fuselage which are not aerodynamically good. The fuselage integrated antenna array is different from the conformal arrays. Here, the antenna layer is structurally integrated within the fuselage layer of the aircraft such that the fuselage becomes a multi-functional structure as antenna structure as well as the fuselage structure of the aircraft. The major advantage of this approach is that the higher profile antenna arrays (as thick as the fuselage) can be installed on an aircraft without creating protrusions on the fuselage. The dorsal and side-mounted antennas do not require major modifications to the fuselage. In contrast, a fuselage integrated antenna requires co-designing the fuselage jointly with the

antenna. Hence, the aerodynamic performance of the aircraft and antenna structure must be co-optimized. The present antenna design in this paper was carried out by taking into account this co-optimization though the final fuselage integrated antenna system has not been completed.

B. SANDWICH STRUCTURE

Fig. 2 shows the basic drawing of a sandwich structure. It is composed of two thin stiff face sheets bonded to a thick honeycomb or foam core material. Due to its high stiffness-to-weight ratio, significant uses of sandwich structures can be found in the constructions of aircraft and spacecraft structures [19]. A sandwich structured antenna array would give the antenna high rigidity and mechanical strength with reduced weight, hence, fulfilling the mechanical properties needed for a load-carrying fuselage and electrical requirements of the antenna array. The sandwich structured antenna arrays such as [20], [21] shows great promise for the multi-disciplinary design of a structurally integrated antenna. Note that the antennas in [20], [21] have fixed beam direction, no scanning functions.

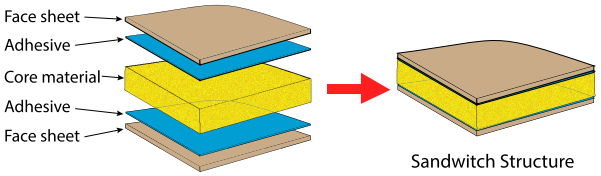

FIGURE 2. Basic schematic view of sandwich structure.

C. DESIGN GOALS AND CONSIDERATIONS

The specific design goals of this work are:

1) Design a large wide-scanning horizontally-polarized phased-array antenna operating at S-band (2-4 GHz).
2) The array should comprise 200 × 20 (azimuth × elevation) elements while enabling the integration in the fuselage in the form of a sandwich-structured composite.
3) The structure-integrated design should be capable of enduring very tough environmental conditions, such as high wind pressure, high static loads, high bending moment and large operating temperature range.
4) Design trade-off consideration: It is worth mentioning that wide scanning and good mechanical integration are more important than wide bandwidth for the targeted application.

The requirements for the active reflection coefficient ($|\Gamma_{act}|$) and relative bandwidth of the array are given in Table 1. Designing an antenna array simultaneously for low element height, wide scan range, wide bandwidth and good input matching is very difficult due to the fundamental trade-off between these parameters [5]. Therefore, the $|\Gamma_{act}|$ for 25% bandwidth is relaxed to −5 dB level. The targeted application of this antenna array design is Airborne Early Warning (AEW) aircraft such as Saab Erieye [16]. Such antenna sensors should have 10% bandwidth for long-range target detection and 25% bandwidth for close-range electronic warfare. Since electronic warfare occurs at a much closer range and the antenna directivity will remain the same (antenna size is the same), we can afford to have higher reflections at antenna input for 25% bandwidth. Hence, this specification is due to the specific application requirement of the project. Azimuth scanning of ± 75° is desired to achieve a large coverage area whereas elevation scanning of ±15° is desired to detect ground and air targets. Additionally, the antenna radiation efficiency (η_{rad}) ≥ 95% and the sidelobe level of −13 dB relative to the main lobe is desired for the large antenna array, (200 × 20 element array).

TABLE 1. Electrical design goals of the antenna array.

Bandwidth	$\|\Gamma_{act}\|$	Scan range
10%	-10 dB	±75° (azimuth) ±15° (elevation)
25%	-5 dB	±75° (azimuth) ±15° (elevation)

Although the primary goal is to verify the electrical performance of the selected antenna element (without the sandwich material, radome, stringers and fixtures), the structure integration considerations are included as additional design constraints. These design considerations are listed below:

1) The antenna array shall have a ground plane and if PCBs are employed, they should be able to bond to a honeycomb or foam core material to make a sandwich structure.
2) The sandwich structure core materials such as Kevlar honeycomb and Rohacell foam have very low dielectric constant (in the order of 1 − 1.2). Due to this, the electrical performance of the antenna is assumed to be very similar to that of the one without the core materials.
3) The element height is selected such that the sandwich-structured integrated antenna is of relatively low profile (with height < 0.4λ) but thick enough (30 to 40 mm) such that the fuselage does not lose the required mechanical rigidity by being too thin.
4) The antenna structure should be modular to several sub-apertures so that the total antenna array of 200 × 20 elements can be manufactured in a modular manner with sub-arrays, each consisting of 7 × 7 − 10 × 10 elements.

III. ANTENNA DESIGN

For the above-described application requirements and constraints, the concept of the connected cross bowtie antenna element is selected, which has been recently introduced by the authors in [22] and further elaborated in this work. Fig. 3 shows a unitcell of the connected cross bowtie antenna element, including its cross-section. The PCB layers of the unitcell element are shown in Fig. 4. The antenna element is composed of two orthogonal bowtie elements etched on

the bottom layer of the PCB substrate and placed above the ground plane, supported by one solid pillar and one hollow pillar. A standard two-hole flange SMA connector with extended PTFE dielectric and the inner conductor is inserted into the hollow pillar. Diameters of the inner conductor, dielectric and hole of the hollow pillar are chosen in order to realize a 50Ω coaxial feed line. The hollow pillar is connected to the ground plane at one end and at the other end to one of the arms of a bowtie element. The inner conductor of the coaxial feed line is connected to the other arm of the same bowtie using a microstrip line on the top layer of the PCB. A solid pillar is also connected to this other arm of the bowtie on the bottom layer of the PCB at one end and the ground plane at the other end. The unitcell has the volume of $d_x \times d_y \times d_z = 0.4\lambda \times 0.4\lambda \times 0.34\lambda$, where λ corresponds to the wavelength in free-space at 3 GHz.

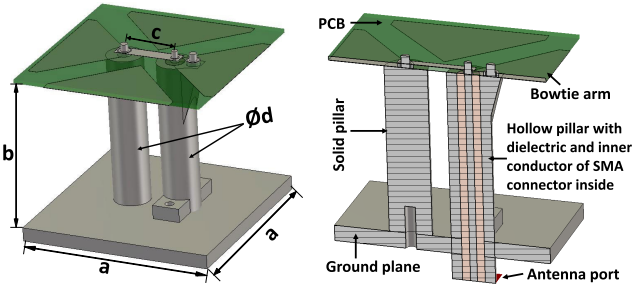

(a) extended view (b) cross-section view

FIGURE 3. Unitcell of antenna element.

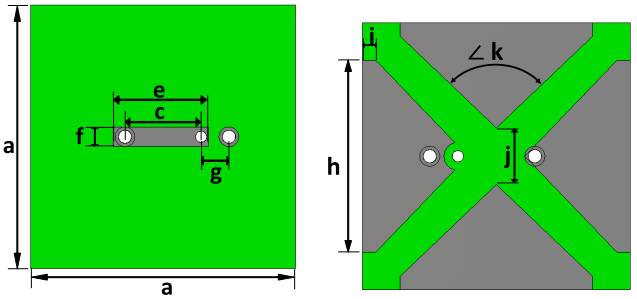

(a) upside (b) underside

FIGURE 4. Unitcell of radiation element realized by single-layer PCB.

TABLE 2. Optimized geometrical parameter values of the cross bowtie antenna element as defined in Figs. 3 and 4.

Parameter	Value [mm]	Parameter	Value [mm]
a	40	h	28.8
b	32.5	i	2
c	11.5	j	8.5
d	8	α	92.5°
e	14.4	D_i^*	1.3
f	3	D_o^*	4.2
g	4.2		

* Parameters D_i and D_o are diameters of inner conductor and dielectric layer of the extended SMA connector.

The hollow and solid pillars together with the SMA connector with extended dielectric and inner conductor, represent a folded balun structure that transforms the single-ended antenna input port to the differential pairs of the bowties ports. The transition from the pillars to the PCB is realized through the pin structures on the top of the pillars (see Figs. 3 and 7). The pins go through the plated via-holes and are soldered to the pads of the plated via-holes on the PCB top layer. If dual polarization is desired, one can configure the second bowtie with a pair of hollow and solid pillars, similar to the single polarized bowtie as shown in [22]. It is worth mentioning that removing the second bowtie reduces the bandwidth of the unitcell antenna element of single-polarization as in this work. Therefore, even though only the horizontal polarization is required for the considered application, the second bowtie is still present in the element design in this work without significant extra cost.

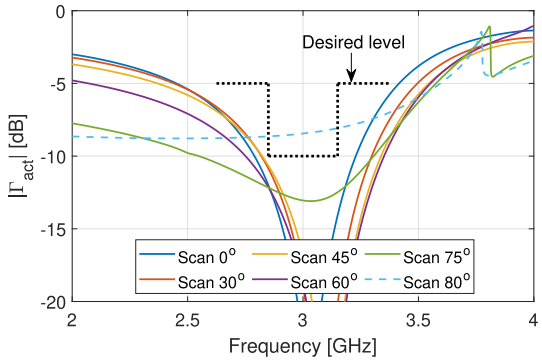

(a) 0° elevation

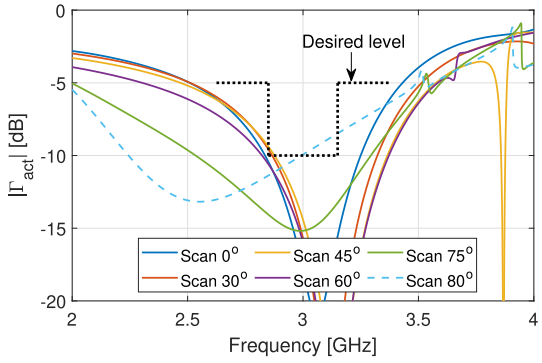

(b) 15° elevation

FIGURE 5. Simulated $|\Gamma_{act}|$ of unitcell of antenna element in infinite array environment at various azimuth directions.

The antenna element was optimized under the infinite array condition with the goal to meet the specification in Table 1. The resultant design parameters are summarized in Table 2. Fig. 5 presents the active reflection coefficient ($|\Gamma_{act}|$) of the connected cross bowtie element in the infinitely large array at various azimuth directions for both 0° and 15° elevations. As seen, they are within the desired levels, i.e. $|\Gamma_{act}| < -10$ dB and < -5 dB over the bandwidth of 10% and 25%, respectively, up to the scan angles of ±75°.

The element is also capable to scan up to azimuth ±80° and elevation ±15° with the $|\Gamma_{act}| < -8$ dB for the 10% and 25% bandwidth.

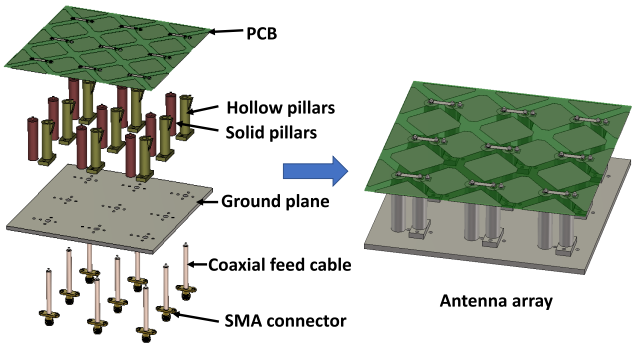

FIGURE 6. Array assembly: (left) manufactured parts and (right) final assembly.

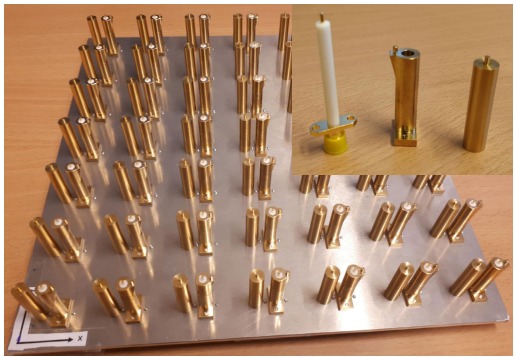

FIGURE 7. Ground plane and pillars of the prototype. View at top right corner shows a set of SMA connector with extended dielectric and inner conductor (left), hollow pillar (center) and solid pillar (right).

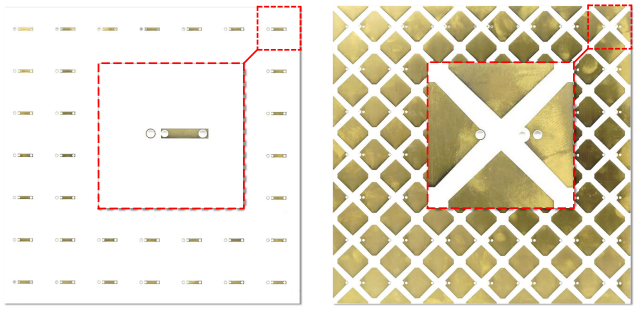

(a) feeding lines on upside (b) cross bowties on underside

FIGURE 8. PCB based radiation element structure.

A finite array of 7×7 such connected cross bowtie antenna elements has been manufactured to verify the element design and analyze the manufacturing and assembly aspects. The ground plane and pillars were manufactured by using the milling technique and the PCB by using the standard PCB etching technique. The ground plane is made of aluminium to enable lightweight (for the final array antenna, the ground plane can be realized even by a thin metal mesh grid sheet on composite material to have a very light and strong structure), and the pillars are made of copper to allow for easier soldering (for the final array antenna, the pillars can also be made of the aluminium and the PCB can be screwed into the pillars using small screws to remove the soldering process). The PCB substrate is 0.8 mm thick Rogers 4350B. The ground plane and the PCB were manufactured as a full piece of structure for the array, whereas the hollow and solid pillars were manufactured individually. The solid and hollow pillars along with the SMA connector were assembled with the ground plane by using screws, then the PCB was placed on the top of it, and the pins on the top of the pillars and the inner conductor of the SMA connector were soldered to the PCB (see Fig. 6). Fig. 7 shows the ground plane and the pillars structure as well as a set of the SMA connector, the hollow pillar and the solid pillar. Fig. 8 illustrates the top and bottom layers of the manufactured PCB. Fig. 9 presents the 7×7 element array prototype.

FIGURE 9. 7 × 7 connected cross bowtie array prototype.

IV. MONTE-CARLO TOLERANCE ANALYSIS

The ground plane and pillars structure were manufactured within ISO 2768-mk[1] tolerance requirement. The manufacturing tolerances of the PCB are very small (copper pattern tolerance is ±50 μm) and it would not negatively affect the performance of the antenna at the S-band. The uncertainties of the antenna performance mainly come from the milling of the ground plane and pillars as well as the assembly of the antenna array. The manufacturing and alignment tolerances were studied using Monte-Carlo simulations in the infinite array scenario. The parameters used in this analysis are given in Table 3.

The smallest mesh-cell used in the CST studio suite at 3 GHz is 0.035 mm. The tolerance values were set to have random uniform distribution with the step of 0.05 mm for all the parameters listed in Table 3, and 1000 different cases of the antenna element with the uniformly distributed independent random tolerances were simulated for each of the following azimuth scan angles: 0°, 45°, 60° and 75° at elevation 0°. Cumulative distribution functions (CDF) of the maximum value of the active reflection coefficient ($|\Gamma_{act}|$)

[1]International Organization for Standardization (ISO) 2768 General geometric tolerances for dimensions without individual tolerance indications.

TABLE 3. Parameters, their values and tolerances used in the Monte-Carlo simulations.

Parameter	Value (mm)	Tolerance (mm)
Solid / hollow pillar height	32.5	± 0.3
Solid / hollow pillar diameter	8	± 0.2
Hollow pillar hole diameter	4.2	± 0.1
Distance between the pillars	11.5	± 0.5
Deviation in the pillars distance due to pillars tilt (at PCB)	0	± 0.5
Element spacing in E- / H-plane	40	± 0.3

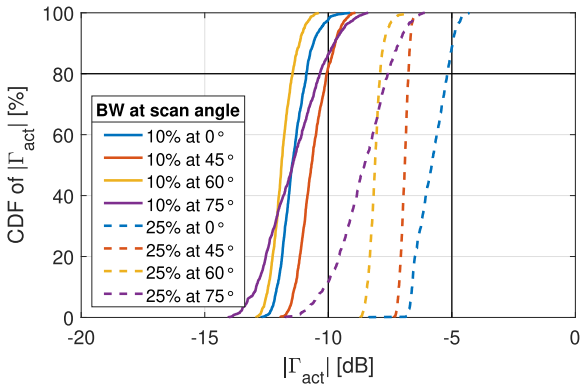

FIGURE 10. Cumulative distribution function (CDF) of maximum $|\Gamma_{act}|$ within 10% and 25% bandwidth when azimuth scan angle at 0°, 45°, 60° and 75°, respectively, and elevation angle at 0°.

within 10% and 25% bandwidth are presented in Fig. 10. It demonstrates the probability of 80% and higher for achieving the specifications in Table 1 within the beam scan range of ±75°. The antenna element was not studied using Monte-Carlo tolerance analysis at elevation 15°. However, we expect that it will give us a similar result at elevation 15°.

The random uniform distribution for the tolerances was selected to have a margin for securing the high possibility of fulfilling the specifications. In practice, the tolerances have a normal distribution where most of the samples have values closer to the values of the parameters than the extreme tolerance values. Therefore, the yield of the antenna element with the desired active reflection coefficient (Γ_{act}) should be better than 80%. The tolerance analysis has not been carried out for the finite array prototype due to the lack of computational resources to simulate large samples of the 7×7 element array. But we believe that the infinite array model for tolerance analysis is not a bad approximation.

V. EXPERIMENTAL RESULTS

Scattering parameters and embedded radiation patterns in E- and H-planes of all elements of the array antenna prototype were measured in the anechoic chamber at Chalmers University of Technology, Gothenburg, Sweden. The embedded element patterns were also measured in an anechoic chamber at Saab AB for cross verification. The element embedded radiation patterns were measured by exciting one element at a time while terminating the other elements with matched 50Ω loads. The active reflection coefficient $\Gamma_{act}(n)$ of the n^{th} element and the far-field function $\mathbf{G}(\theta, \varphi)$ of the whole 7×7 array antenna were obtained through post-processing using (1) and (2) respectively as

$$\Gamma_{act}(n) = \frac{1}{|a_n|} \sum_{m=1}^{M} S_{nm} a_m, M = 49, \quad n = 1, \cdots, 49 \quad (1)$$

$$\mathbf{G}(\theta, \varphi) = \sum_{m=1}^{M} a_m \mathbf{G}_m(\theta, \varphi) e^{jk\mathbf{r}_m \cdot \hat{\mathbf{r}}}, \quad M = 49 \quad (2)$$

where $a_n = |a_n| e^{j\Phi_n}$ is the port excitation at the n^{th} element, S_{nm} the S parameter from element m to element n, $\mathbf{G}_m(\theta, \varphi)$ the embedded far-field function of the m^{th} element, $\mathbf{r}_m$ the location of the m^{th} element, and k the wavenumber. Herein, we considered the port excitations of uniform amplitude distribution with a progressive linear phase to steer the main beam to different directions. Note that due to the limited measurement resource, we measured only the E- and H-plane radiation patterns for the embedded far-field functions of all elements. Therefore, the radiation patterns of the antenna array when scanning at various azimuth directions in elevation angle 0° were calculated directly from eq. 2, whereas the radiation patterns, when scanning at various azimuth directions in elevation angle 15° were estimated using the Body-of-Revolution (BOR) antenna concept (discussed in detail later in the paper).

Fig. 11 demonstrates a good agreement between the simulated and measured coupling coefficients (S parameters) for the central element. As expected, the mutual couplings are stronger in the horizontal direction than in the vertical one because the elements are connected horizontally. It is also worth noting that the array is symmetric in the vertical axis but asymmetric in the horizontal axis due to asymmetric feeding structure (see the solid and hollow pillars in Fig. 3).

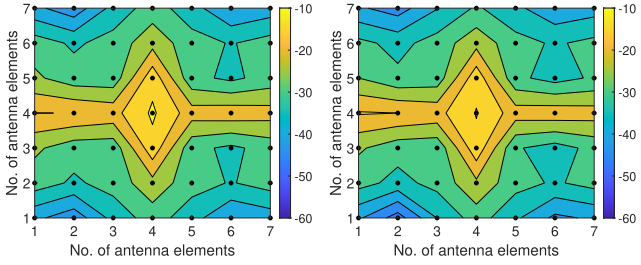

(a) simulation (b) measurement

FIGURE 11. Magnitude of mutual coupling coefficients between the central element and other elements in the 7 × 7 array prototype. The black dots represent locations of antenna elements' center.

Figs. 12 and 13 illustrate that the measured and simulated active reflection coefficients ($|\Gamma_{act}|$) of the central element of the antenna array are in good agreement when scanning at elevation angles 0° (Fig. 12) and 15° (Fig. 13) and azimuth angles 0°, 30°, 45° and 60°. Fig. 14 presents $|\Gamma_{act}|$ of the central and its eight adjacent elements of the antenna array when scanning at elevation angles 0° and 15° and azimuth angles 0°, 30°, 45° and 60° in a Smith Chart. As seen, the

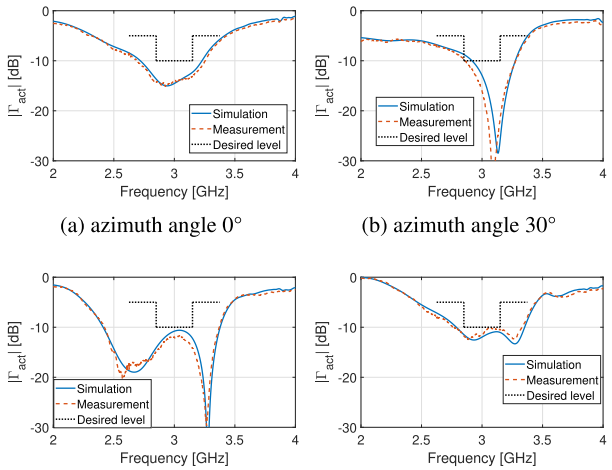

(a) azimuth angle 0° (b) azimuth angle 30°

(c) azimuth angle 45° (d) azimuth angle 60°

FIGURE 12. $|\Gamma_{act}|$ of central element of the prototype when scanning at elevation angle 0° and different azimuth angles.

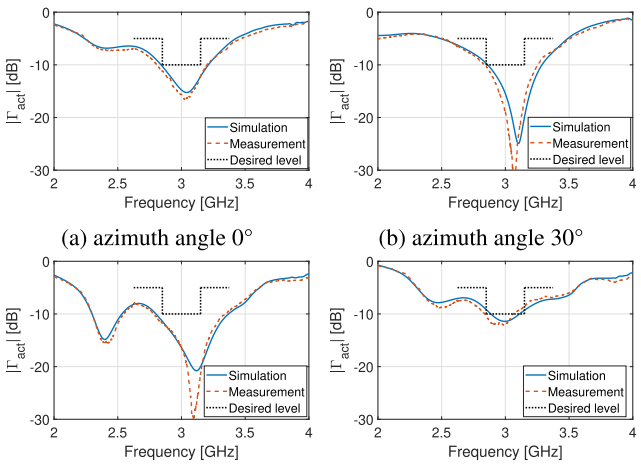

(a) azimuth angle 0° (b) azimuth angle 30°

(c) azimuth angle 45° (d) azimuth angle 60°

FIGURE 13. $|\Gamma_{act}|$ of central element of the prototype when scanning at elevation angle 15° and different azimuth angles.

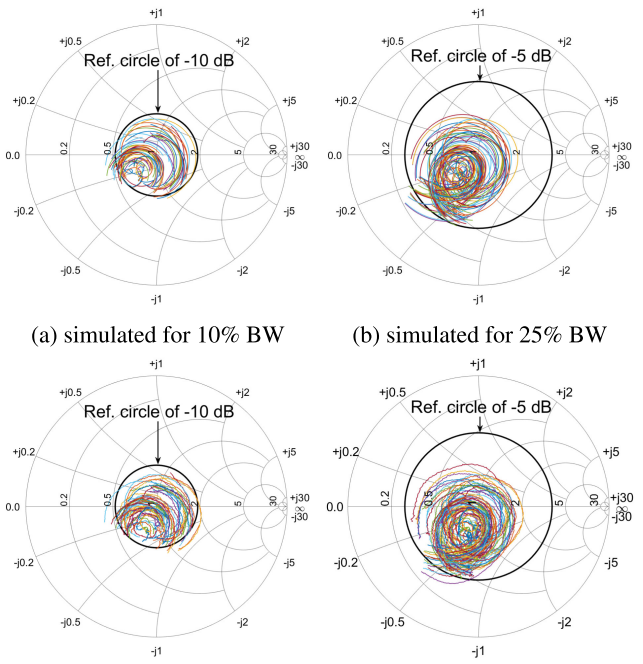

(a) simulated for 10% BW (b) simulated for 25% BW

(c) measured for 10% BW (d) measured for 25% BW

FIGURE 14. $|\Gamma_{act}|$ of central element and its eight adjacent elements of the prototype for different bandwidth (BW) when scanning at azimuth angles 0°, 30°, 45° and 60° at both elevation angles 0° and 15°.

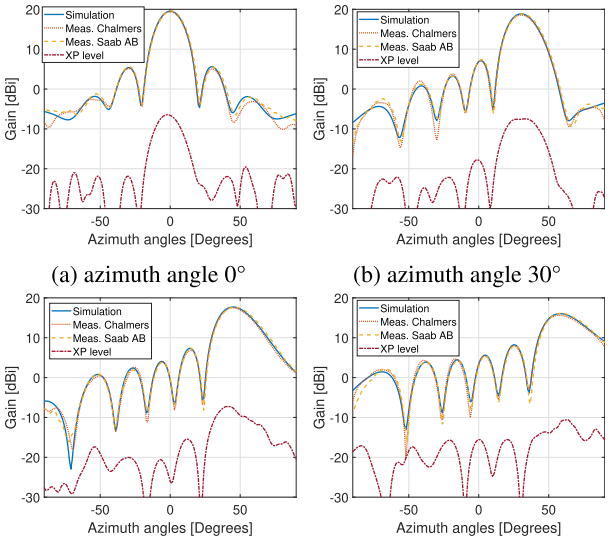

(a) azimuth angle 0° (b) azimuth angle 30°

(c) azimuth angle 45° (d) azimuth angle 60°

FIGURE 15. Radiation patterns of the prototype when scanning at the elevation angle 0° and different azimuth angles at 3 GHz.

simulated and measured $|\Gamma_{act}|$ curves have similar behavior and are mostly within the −10 dB and −5 dB reference black circles within 10% and 25% bandwidth, respectively. Figs. 12–14 show that the 7 × 7 element array prototype is capable of steering beam up to ±60° with the active reflection coefficient below −10 dB and −5 dB for the bandwidth of 10% and 25% respectively. This is the desired active reflection coefficient levels for the targeted application as shown in the specification in Table 1.

Fig. 15 shows the total radiation patterns of the antenna array prototype when scanning at elevation angle 0° and azimuth angles 0°, 30°, 45° and 60°. Notations "Meas. Chalmers" and "Meas. Saab AB" represent the data based on the embedded element patterns measured at Chalmers and Saab AB, respectively. The simulated and measured results agree well. The maximum relative cross-polar level is below −25 dB for all beam scan directions. The first sidelobe level when the main beam at azimuth 0° (at broadside) is −13.29 dB relative to the peak of the main lobe. The sidelobe level is as expected since, according to the antenna theory, a rectangular aperture phased array antenna with uniform amplitude excitation has the first sidelobe relative level of −13.26 dB. When scanning at wider scan angles, the sidelobe

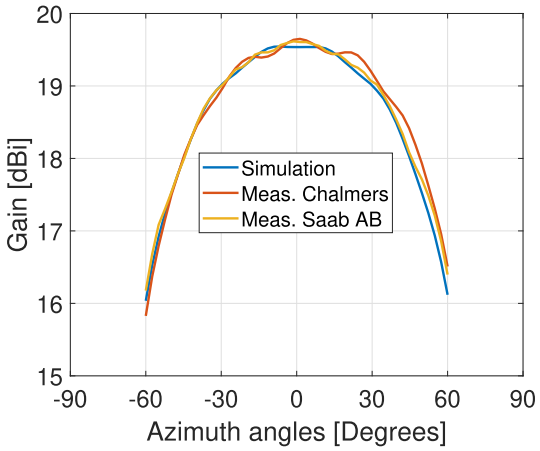

FIGURE 16. Main beam gain of the prototype at 3 GHz versus azimuth scan angles with elevation angle 0°.

level increases primarily due to the edge effects that make the aperture distribution different from the expected uniform distribution, and when the main beam is steered to azimuth angle 60° the sidelobe relative level of the 7 × 7 elements antenna prototype is −8.07 dB, 5 dB higher than that with a broadside main beam. The sidelobe levels at wide scan angles can be lowered by using a larger antenna array because in a larger array the edge effects will be smaller and the aperture distribution will be close to the uniform distribution. This can be seen in Fig. 21, where the simulated sidelobe levels of the 200 × 20 elements antenna array is −13.26 dB and −12.91 dB with broadside main beam and azimuth 80° main beam, respectively. Another way of decreasing the sidelobe level is to use amplitude tapering in the antenna array excitation, which at the same time further reduces the edge effects. Another observation in Fig. 15 is that the far-out sidelobes are slightly different between the two measurements. This difference is quite small and presumed to be caused by the anechoic chamber measurement uncertainties.

Fig. 16 shows the gain variation of the prototype when the main beam is at different azimuth scan angles with fixed elevation angle 0°. Herein, we can see that the simulated and measured gain values match well. The gain with the broadside beam is 19.53 dBi. The gain decreases with scan angle increase and the scan loss (reduction of the gain when scanning) is 3.5 dB when beam scanned at ±60°. For comparison, an infinitely large uniformly excited phased array of ideal isotropic antenna elements with the element spacing of $\lambda/2$ would have the scan loss of $-10\log(\cos(60°)) = 3$ dB when scanning at 60°. The extra 0.5 dB scan loss is mainly caused by the edge effects of the array due to its small size. One can also notice that there are ripples in the measured gain values especially when scanning at the ±15° sector and especially in Meas. Chalmers. However, these ripple values are small (<0.17 dB) for Meas. Chalmers and they are even smaller (< 0.06 dB) for Meas. Saab AB (which was done in a larger anechoic chamber than that of Meas. Chalmers). We presumed that these ripples are caused by reflections from the absorbers in the anechoic chamber adding up constructively or destructively, and the ripples are smoother in Meas. Saab AB because a larger anechoic chamber means lower power is reflected back to the antenna array from the absorbing walls.

The radiation efficiency of the antenna array is higher than 95% across all scan angles (i.e. azimuth ±60° and elevation ±15°) within the bandwidth of interest. Hence, antenna efficiency (defined as the ratio of total radiated power to the total input power) is mainly dominated by the active reflection coefficients ($|\Gamma_{act}|$) at the antenna element input ports.

Due to the limited measurement resource, we only measured the E- and H-plane embedded radiation patterns of each element of the prototype. Therefore, the radiation patterns of the whole prototype antenna when the main beam is steered at elevation angle 15° cannot be obtained by post-processing with only (2). Nevertheless, the purposed bowtie antenna element is a dipole type antenna, whose performance is very close to that of a BOR1 (Body-of-Revolution type 1) antenna and we can estimate the radiation pattern at elevation angle 15° by using the well-established BOR1 approximation method [23]. First, the total E- and H-patterns of the antenna array were calculated using (2). The corresponding θ and φ angles for a given azimuth angle (az) and elevation angle (el) was found using (3). Then the co- and xp-polar patterns at φ-plane was determined by (4) and finally, the radiation pattern was transformed from spherical coordinate system to Ludwig 2 (azimuth/elevation) using (5) [24]. Fig. 17 shows the co-polar radiation patterns of the prototype when the main beam scanned at elevation angle 15° and azimuth angles 0°, 30°, 45° and 60°. Notations ''Simulated (true pattern)'', ''Simulated (BOR1 pattern)'' and ''Measured (BOR1 pattern)'' represents the pattern obtained from the simulated 3D radiation pattern, the pattern which was derived by BOR1 theory using simulated E- and H-plane patterns and the pattern which was derived by BOR1 theory using measured E- and H-plane patterns. One can notice that there is an excellent agreement between the simulated BOR1 pattern, the measured BOR1 pattern and the true 3D simulated far-field pattern though the agreement decreases slightly at azimuth angles 45° and 60°. It occurs mainly because the edge elements in the array behave less like BOR1 antenna and at wide scan angles, the effect of edge elements in the radiation pattern increases. The phase patterns in Fig. 18 also show a good agreement between the exact patterns. The relative difference between the far-field patterns cuts as simulated directly via the 3D pattern analysis (using CST FIT solver) and derived from the measured and simulated E- and H-plane patterns using BOR1 method does not exceed ±0.5 dB and ±6° within the ±10° beam steering range.

$$\begin{aligned} \tan\varphi &= \tan el / \sin az, \\ \cos\theta &= \cos el \cos az, \end{aligned} \tag{3}$$

$$\begin{aligned} \mathbf{G}_{co}(\theta,\varphi) &= \mathbf{G}_{co_{45°}}(\theta) - \mathbf{G}_{xp_{45°}}(\theta)\cos 2\varphi, \\ \mathbf{G}_{xp}(\theta,\varphi) &= \mathbf{G}_{xp_{45°}}(\theta)\sin 2\varphi, \end{aligned} \tag{4}$$

where

$$\mathbf{G}_{co_{45^\circ}}(\theta) = \frac{1}{2}[\mathbf{G}_E(\theta) + \mathbf{G}_H(\theta)],$$
$$\mathbf{G}_{xp_{45^\circ}}(\theta) = \frac{1}{2}[\mathbf{G}_E(\theta) - \mathbf{G}_H(\theta)],$$
$$\mathbf{G}_{az}(az, el) = \frac{\cos\varphi}{\sqrt{1-(\sin\theta\sin\varphi)^2}}\mathbf{G}_{co}(\theta,\varphi) - \frac{\cos\theta\sin\varphi}{\sqrt{1-(\sin\theta\sin\varphi)^2}}\mathbf{G}_{xp}(\theta,\varphi) \quad (5)$$

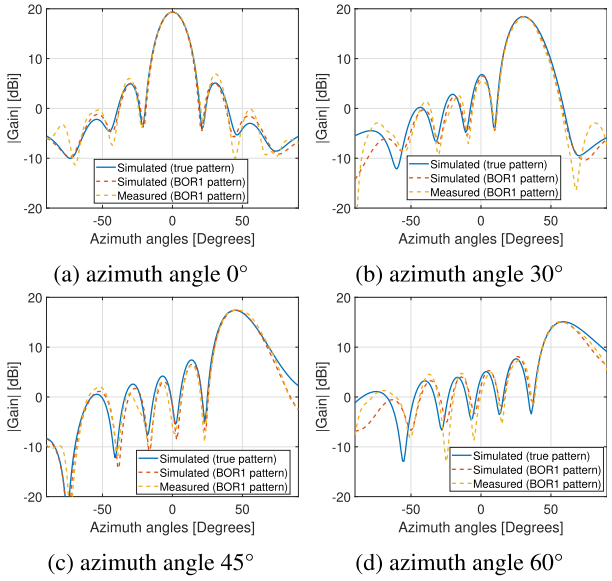

(a) azimuth angle 0° (b) azimuth angle 30°

(c) azimuth angle 45° (d) azimuth angle 60°

FIGURE 17. Amplitude of the radiation patterns of the prototype when scanning at the elevation angle 15° and different azimuth angles at 3 GHz.

Fig. 19 shows the active reflection coefficient and the radiation pattern of the prototype 7 × 7 elements array when scanning at the azimuth angle 75°. It is not as good as that of the infinite array due to the edge truncation effects, as expected. The edge truncation effects of the connected cross bowtie antenna array were studied in [26]. The study has shown that a 7 × 7 element array of such elements cannot scan beyond ± 60° with the performance specified in Table 1. When scanning beyond ±60°, the 7 × 7 elements array prototype have higher active reflection coefficients and higher sidelobe levels than the desired (see Fig. 19). In order to scan at wider angles, one needs either a larger antenna array or employ dedicated means for reducing-edge truncation effects. A larger antenna array of 21 × 7 elements was simulated by using two alternative numerical methods (i.e., CST FIT and HFSS FDTD) for cross verification. Fig. 20 shows that the 21 × 7 element antenna array is capable of fulfilling the desired active reflection coefficient and radiation pattern when scanning at the azimuth 75°.

Due to the big cost of prototyping a full 200 × 20 element array, only the simulated results of the aimed 200×20 element array under the periodic boundary condition are presented in this paper. Fig. 21 shows the simulated radiation patterns of

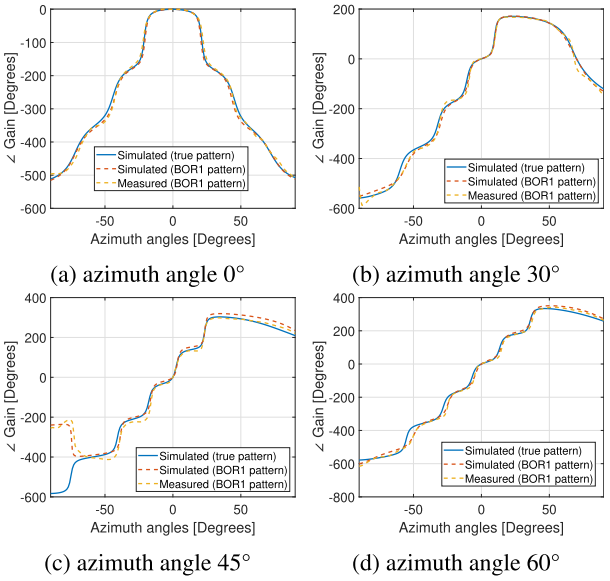

(a) azimuth angle 0° (b) azimuth angle 30°

(c) azimuth angle 45° (d) azimuth angle 60°

FIGURE 18. Phase distribution of the radiation patterns of the prototype when scanning at the elevation angle 15° and different azimuth angles at 3 GHz.

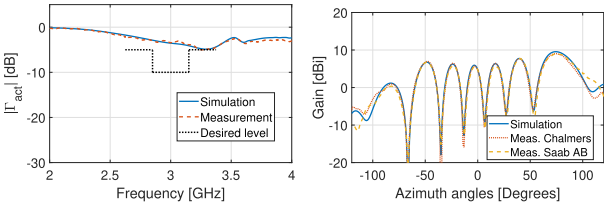

(a) (b)

FIGURE 19. (a) $|\Gamma_{act}|$ of the central element in the array and (b) the radiation pattern of the 7 × 7 element array when scanning at the elevation angle 0° and the azimuth angle 75° at 3 GHz.

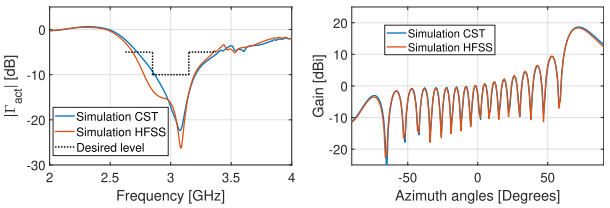

(a) (b)

FIGURE 20. (a) $|\Gamma_{act}|$ of the central element in the array and (b) the radiation pattern of the 21 × 7 element array when scanning at the elevation angle 0° and the azimuth angle 75° at 3 GHz.

the full array. The sidelobe levels are about 13 dB below the main lobe, as expected from the antenna theory. It is good to notice that, even though the simulated radiation performance allows the array scanned up to ±80° off the broadside (see Fig. 21), the simulated active reflection coefficients allows the array scanned up to only ±75° (see Fig. 5).

Fig. 22 shows a comparison of the antenna element height and their maximum scan range in an infinitely large array for various wide scanning planner antenna arrays in the literature. It shows the purposed array antenna (Notation with "Present work") has a lower profile and has a wider scanning range compared to others. Table 4 compares the

TABLE 4. Performance comparison of wide-scanning array antennas.

Antenna element type	No. of array elements	Central Frequency [GHz]	Bandwidth @ $\Gamma_{act} < -10$ dB [%]	Element height [λ at f_{min}]	Scan range [°]	Suitability for the composite sandwich structure fuselage integration [Good/Poor]. Why?
Connected TSA, [1]	8×7	1.15	44	0.9	± 45	Poor. Long element height.
Multi-mode TSA, [9]	$\infty \times \infty$ [1]	1.5	20	1.3	± 80	Poor. Long element height.
Connected dipole, [13]	7×7	4.5	23	0.3	± 45	Poor. Not compatible with sandwich concept.
Cavity backed slot, [25]	18×2	11	14	0.3	± 70	Poor. Very thick and heavy PCB at S-band.
Connected cross bowtie (this work)	21×7 [1]	3	10	0.3	± 75	Good. Have required element height and compatible with sandwich concept.
	7×7				± 60	

[1] Simulation results only.

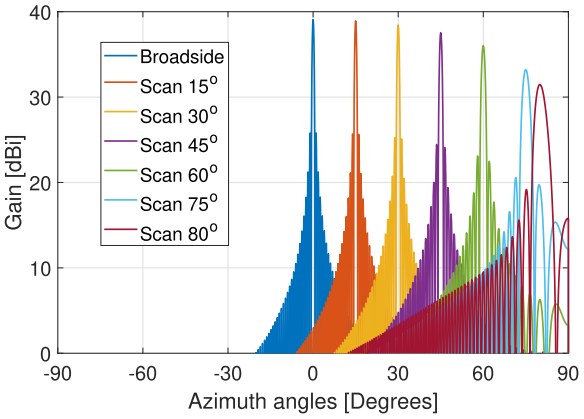

FIGURE 21. Simulated co-polar radiation patterns of aimed 200 × 20 element cross bowtie array antenna with elevation angle 0° and different azimuth angles of 0°, 30°, 45° and 60° at 3 GHz.

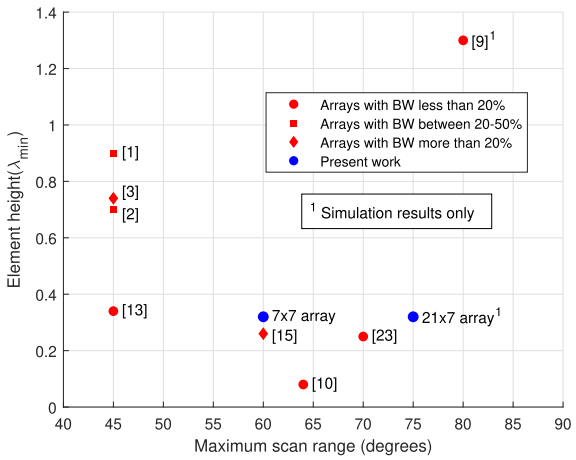

FIGURE 22. Comparing antenna element height and the maximum scan range in an infinitely large array for various antenna arrays in the literature.

key results of the present work with some of the designs shown in Fig. 22. Connected TSA array [1] and multi-mode TSA array [9] have good performance but are not suitable for the desired application due to element height exceeding the required 0.4λ. Most of the reported TSA arrays in literature have element height of at least 1λ for good performance, including [1], [9]. Connected dipole array in [13] has desired element height and relatively simple design but it can only steer the beam to ±45° and its geometry is not compatible with the sandwich structure integration. On the other hand, the connected cavity-backed slot array [25] does have wide-scanning capabilities. However, they are made of multiple PCB structures at X-band. At S-band the PCB type of arrays will be very heavy and fragile to vibration due to full dielectric substrate. Hence, they are not suitable for fuselage integration. We should note that the wide scanning range and good mechanical integration are more important than the wide bandwidth for the targeted application. Apart from the multi-mode TSA [9], all other antenna arrays in Table 4 have a smaller scanning range than the required for the targeted application. In Table 4, the bandwidth is given for active reflection coefficient $\Gamma_{act} < -10$ dB when beam steered from broadside to their maximum steering angle. Hence, even if we look at a smaller bandwidth, the scan range of these arrays will not increase at $\Gamma_{act} < -10$ dB level. Additionally, previously published fuselage integrated sandwich antenna structures like [20], [21] had been designed with mechanical constraints required for the aeronautical applications but had no electronic beam scanning capabilities. The proposed connected bowtie antenna array has advantages over the previous designs in satisfying the challenging combination of requirements for the impedance bandwidth and scan range while respecting the mechanical constraints of the targeted application.

VI. CONCLUSION

The compatibility to structure integration as a sandwich-structured fuselage-integrated antenna array application severely limits the range of possible antenna array solutions that can enable a wide scan range over a reasonable bandwidth. Most reported previous designs have common disadvantages in that they are not compatible for sandwich-structured fuselage integrated array, which has been overcome in this work by a new antenna array design consisting of connected cross-bowtie antenna elements.

The proposed antenna array of connected cross bowtie elements represents a good candidate for a low-profile sandwich-structured fuselage-integrated antenna array. When the number of array elements is large (tending to infinity), it is theoretically capable of beam scanning grating-lobe-free up to ±75° in the azimuth and ±15° in the elevation off the broadside direction over the 10% and 25% bandwidth with the active reflection coefficient $\Gamma_{act} < -10$ dB and −5 dB, respectively. A statistical analysis of manufacturing and assembly tolerances including the critical interfaces (e.g. at the element, feed, and ground plane) shows promising

results, with over 80% probability to achieve the desired performance according to the ISO 2768-mk standard tolerances. Measurements of a small-size array prototype consisting of 7×7 cross bowtie connected elements are in good agreement with the simulated results. The antenna prototype has been verified being able to provide a $[-60°, 60°]$ azimuth scan range for $[-15°, 15°]$ elevation scan range while complying with the mechanical design constraints for structure integration (including the element height of 0.35λ, mechanical rigidness, and scalability to large arrays of sub-array modules).

REFERENCES

[1] R. Maaskant, M. V. Ivashina, O. Iupikov, E. A. Redkina, S. Kasturi, and D. H. Schaubert, "Analysis of large microstrip-fed tapered slot antenna arrays by combining electrodynamic and quasi-static field models," *IEEE Trans. Antennas Propag.*, vol. 59, no. 6, pp. 1798–1807, Jun. 2011.

[2] E. de Lera Acedo, E. Garcia, V. González-Posadas, J. L. Vazquez-Roy, R. Maaskant, and D. Segovia, "Study and design of a differentially-fed tapered slot antenna array," *IEEE Trans. Antennas Propag.*, vol. 58, no. 1, pp. 68–78, Jan. 2010.

[3] T.-H. Chio and D. H. Schaubert, "Parameter study and design of wide-band widescan dual-polarized tapered slot antenna arrays," *IEEE Trans. Antennas Propag.*, vol. 48, no. 6, pp. 879–886, Jun. 2000.

[4] H. Holter, "Dual-polarized broadband array antenna with BOR-elements, mechanical design and measurements," *IEEE Trans. Antennas Propag.*, vol. 55, no. 2, pp. 305–312, Feb. 2007.

[5] B. L. G. Jonsson, C. I. Kolitsidas, and N. Hussain, "Array antenna limitations," *IEEE Antennas Wireless Propag. Lett.*, vol. 12, pp. 1539–1542, 2013.

[6] A. Ludvig-Osipov, J.-M. Hannula, P. Naccachian, and B. L. G. Jonsson, "Physical limitations of phased array antennas," 2020, *arXiv:2006.02777*. [Online]. Available: http://arxiv.org/abs/2006.02777

[7] C.-M. Liu, S.-Q. Xiao, H.-L. Tu, and Z. Ding, "Wide-angle scanning low profile phased array antenna based on a novel magnetic dipole," *IEEE Trans. Antennas Propag.*, vol. 65, no. 3, pp. 1151–1162, Mar. 2017.

[8] D. S. Prinsloo, P. Meyer, R. Maaskant, and M. V. Ivashina, "Conical quad-mode antenna with integrated tapered slot antennas for wide-field polarimetry," in *Proc. IEEE-APS Top. Conf. Antennas Propag. Wireless Commun. (APWC)*, Sep. 2015, pp. 1235–1238.

[9] M. V. Ivashina, E. Redkina, R. Maaskant, and D. S. Prinsloo, "Capabilities and fundamental limitations of multi-mode antennas in an array environment," in *Proc. 10th Eur. Conf. Antennas Propag. (EuCAP)*, Apr. 2016, pp. 1–4.

[10] G. Gao, X. Ding, Y.-F. Cheng, and W. Shao, "Dual-polarized wide-angle scanning phased array based on mutimode patch elements," *IEEE Antennas Wireless Propag. Lett.*, vol. 18, no. 3, pp. 546–550, Mar. 2019.

[11] S. Xiao, C. Zheng, M. Li, J. Xiong, and B.-Z. Wang, "Varactor-loaded pattern reconfigurable array for wide-angle scanning with low gain fluctuation," *IEEE Trans. Antennas Propag.*, vol. 63, no. 5, pp. 2364–2369, May 2015.

[12] X. Ding, B.-Z. Wang, and G.-Q. He, "Research on a millimeter-wave phased array with wide-angle scanning performance," *IEEE Trans. Antennas Propag.*, vol. 61, no. 10, pp. 5319–5324, Oct. 2013.

[13] D. Cavallo, A. Neto, G. Gerini, A. Micco, and V. Galdi, "A 3-to 5-GHz wideband array of connected dipoles with low cross polarization and wide-scan capability," *IEEE Trans. Antennas Propag.*, vol. 61, no. 3, pp. 1148–1154, Mar. 2013.

[14] J. A. Kasemodel, C.-C. Chen, and J. L. Volakis, "Wideband planar array with integrated feed and matching network for wide-angle scanning," *IEEE Trans. Antennas Propag.*, vol. 61, no. 9, pp. 4528–4537, Sep. 2013.

[15] S. M. Moghaddam, J. Yang, and A. U. Zaman, "Fully-planar ultrawideband tightly-coupled array (FPU-TCA) with integrated feed for wide-scanning millimeter-wave applications," *IEEE Trans. Antennas Propag.*, vol. 68, no. 9, pp. 6591–6601, Sep. 2020.

[16] M. Heed, "The ERIEYE phased array antenna-from a systems viewpoint," in *Proc. IEEE Int. Conf. Phased Array Syst. Technol.*, May 2000, pp. 391–394.

[17] C. Loecker, P. Knott, R. Sekora, and S. Algermissen, "Antenna design for a conformal antenna array demonstrator," in *Proc. 6th Eur. Conf. Antennas Propag. (EUCAP)*, Mar. 2012, pp. 151–153.

[18] H. Schippers, J. Verpoorte, P. Jorna, A. Hulzinga, A. Meijerink, C. G. H. Roeloffzen, L. Zhuang, D. A. I. Marpaung, W. van Etten, R. G. Heideman, A. Leinse, A. Borreman, M. Hoekman, and M. Wintels, "Broadband conformal phased array with optical beam forming for airborne satellite communication," in *Proc. IEEE Aerosp. Conf.*, Mar. 2008, pp. 1–17.

[19] F. A. Fazzolari, "Sandwich structures," in *Stability and Vibrations of Thin Walled Composite Structures*, H. Abramovich, Ed. Sawston, U.K.: Woodhead Publishing, 2017, ch. 2, pp. 49–90.

[20] J. Zhou, J. Huang, L. Song, D. Zhang, and Y. Ma, "Electromechanical co-design and experiment of structurally integrated antenna," *Smart Mater. Struct.*, vol. 24, no. 3, Feb. 2015, Art. no. 037004.

[21] C. S. You, W. Hwang, H. C. Park, R. M. Lee, and W. S. Park, "Microstrip antenna for SAR application with composite sandwich construction: Surface-antenna-structure demonstration," *J. Compos. Mater.*, vol. 37, no. 4, pp. 351–364, Feb. 2003.

[22] P. Khanal, J. Yang, M. Ivashina, A. Höök, and R. Luo, "A wide coverage S-Band array with dual polarized connected bowtie antenna elements," in *Proc. IEEE Int. Symp. Antennas Propag. USNC-URSI Radio Sci. Meeting*, Jul. 2019, pp. 2001–2002.

[23] P. S. Kildal, *Foundations of Antenna Engineering*. Gothenburg, Sweden: Kildal Antenna AB, 2015.

[24] A. Ludwig, "The definition of cross polarization," *IEEE Trans. Antennas Propag.*, vol. AP-21, no. 1, pp. 116–119, Jan. 1973.

[25] R.-L. Xia, S.-W. Qu, S. Yang, and Y. Chen, "Wideband wide-scanning phased array with connected backed cavities and parasitic striplines," *IEEE Trans. Antennas Propag.*, vol. 66, no. 4, pp. 1767–1775, Apr. 2018.

[26] P. Khanal, J. Yang, M. Ivashina, A. Höök, and R. Luo, "Edge truncation effects in a wide-scan phased array of connected bowtie antenna elements," in *Proc. 14th Eur. Conf. Antennas Propag. (EuCAP)*, Mar. 2020, pp. 1–5.

PRABHAT KHANAL (Graduate Student Member, IEEE) received the B.S. degree in electrical engineering from the Helsinki Metropolia University of Applied Sciences, Helsinki, Finland, in 2016, and the M.S. degree in electrical engineering from Aalto University, Espoo, Finland, in 2018. He is currently pursuing the Ph.D. degree in electrical engineering with the Chalmers University of Technology, Gothenburg, Sweden. His research interests include wide scanning phased array antennas and their applications.

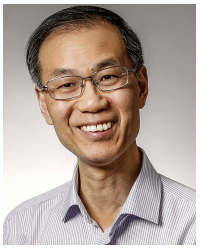

JIAN YANG (Senior Member, IEEE) received the B.S. degree in electrical engineering from the Nanjing University of Science and Technology, Nanjing, China, in 1982, the M.S. degree in electrical engineering from the Nanjing Research Center of Electronic Engineering, Nanjing, in 1985, and the Swedish Licentiate and Ph.D. degrees from the Chalmers University of Technology, Gothenburg, Sweden, in 1998 and 2001, respectively. From 1985 to 1996, he was with the Nanjing Research Institute of Electronics Technology, Nanjing, as a Senior Engineer. From 1999 to 2005, he was with the Department of Electromagnetics, Chalmers University of Technology, as a Research Engineer. From 2005 to 2006, he was with Comhat AB, as a Senior Engineer. From 2006 to 2010, he was an Assistant Professor at the Department of Signals and Systems, Chalmers University of Technology. In 2010, he was an Associate Professor with the Department of Electrical Engineering, Chalmers University of Technology, where he was a Professor, in 2016, and a Full Professor, in 2020. He has published more than 72 journal articles and about 150 peer-reviewed conference papers. H-index: 28. His research interests include ultra-wideband antennas and UWB feeds for reflector antennas, mmWave antennas, mmWave multilayer phased array antennas, mmWave SWE (sheet waveguide element) antennas, gap waveguide antennas, UWB radar systems, UWB antennas in near-field sensing applications, hat-fed antennas, reflector antennas, radome design, and computational electromagnetics.

MARIANNA IVASHINA (Senior Member, IEEE) received the Ph.D. degree in electrical engineering from Sevastopol National Technical University (SNTU), Ukraine, in 2001. From 2001 to 2010, she was with the Netherlands Institute for Radio Astronomy (ASTRON), where she carried out research on innovative phased array technologies for future radio telescopes, such as the square kilometer array. From 2002 to 2003, she also stayed as a Visiting Scientist with the European Space Agency, ESTEC, where she studied multiple-beam array feeds for the satellite telecommunication system large deployable antenna. In January 2011, she joined the Chalmers University of Technology, Gothenburg, Sweden, where is currently a Full Professor and the Head of the Antenna Systems Group, Department of Electrical Engineering. She has published extensively on the above topics, having authored/coauthored over 130 journals and conference papers. Her current research interests include antenna array systems, integration of antennas with active electronic components, synthesis of aperiodic arrays, and other unconventional array architectures, reflector antennas, and focal plane array feeds. She has received several scientific awards, including the URSI Young Scientists Award for GA URSI, Toronto, Canada, in 1999; the APS/IEEE Travel Grant, Davos, Switzerland, in 2000; the Best Team Contribution Paper Award at the ESA Antenna Workshop, in 2008; the EU FP7 Marie Curie Actions International Qualification Fellowship, in 2009; and the Best Paper Award at the IEEE COMCAS Conf., Tel-Aviv, Israel, in 2019; and numerous research project funding grants from Swedish and European funding agencies. She is currently an Associate Editor of the IEEE TRANSACTIONS ON ANTENNAS AND PROPAGATION and a Board Member of the European School of Antennas (ESoA). Since 2021, she has been the Delegate of the European Association of Antennas and Propagation (EurAAP) for Region 6: Iceland, Norway, and Sweden.

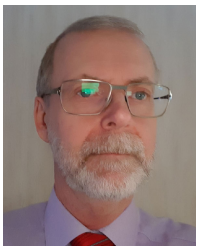

ANDERS HÖÖK received the Ph.D. degree in EM field theory from the Chalmers University of Technology, Gothenburg, Sweden, in 1991. In 1993, he received an Associate Professorship at the Chalmers University of Technology. He is currently a Senior Specialist in sensor technology strategies at Saab AB.

RUOSHAN LUO received the Ph.D. degree in civil engineering from the Chalmers University of Technology, Gothenburg, Sweden, in 1995. She is currently working at Saab AB, Gothenburg, in the areas of structural integrity, environmental requirements, and reliability.